AIAA AVIATION Forum
5-9 June 2017, Denver, Colorado
23rd AIAA/CEAS Aeroacoustics Conference

Jet Noise Simulation Using Ouasi-1D Schemes on Unstructured Meshes

Alexey P. Duben[1] and Tatiana K. Kozubskaya[2]
Keldysh Institute of Applied Mathematics of RAS, Moscow, 125047, Russia

The paper presents a computationally cheap higher-accuracy numerical algorithm applicable to the simulation of jet acoustics on unstructured meshes. In order to predict a distributed noise source presented by a jet, we adapt the hybrid RANS-LES scale-resolving approaches of DES family to unstructured meshes and implement them using the quasi-1D edge-based vertex-centered schemes. To simulate jet far field noise, we use the integration method of Ffowcs-Williams Hawkings. A workability of the resulting "unstructured" algorithm is demonstrated on several cases: subsonic unheated and sonic underexpanded hot jets.

I. Introduction

Due to its significant impact on acoustics of modern aircraft, jet is remaining among the main objects of investigations targeted at the overall noise reduction. It is studied either as an isolated source of sound or as a component which contributes to installation noise. A part of numerical simulation in the research dealing with jet noise reduction constantly grows with the improvements in mathematical models and numerical algorithms along with the rapid development of high-performance computers.

In comparison with jet aerodynamics, jet aeroacoustics is much more sensitive to the accuracy of numerical methods used for the predictions. Thus, high-accuracy schemes are in great demand. Nowadays the choice of high-accuracy numerical method still gravitates toward cheaper algorithms on structured meshes. Most successful predictions of jets are carried out in the framework of structured algorithms. However, the deeper numerical simulations penetrate industrial applications the greater need in unstructured meshes is recognized. This fact is confirmed by a series of recent predictions of jet acoustics which have been performed on unstructured meshes. For instance, the paper of Lupoglazoff&Vuillot[1] presents jet simulations on fully unstructured tetrahedrons-predominantly meshes with the help of second-order MUSCL type scheme using in-house CEDRE code. Tucker et al.[2,3] apply the kinetic-energy preserving numerical scheme on unstructured meshes implemented in the HYDRA code. The first above-mentioned numerical scheme is rather dissipative so, in order to resolve turbulent perturbations and acoustic waves correctly, the authors are forced to carry out the corresponding predictions on huge meshes. The kinetic-energy preserving scheme is low-dissipative nonetheless like MUSCL-type schemes it exploits a compact numerical stencil for interpolation, so the mesh requirements remain quite high. The usage of high-order Discontinuous Galerkin (DG) method allows for rather coarse meshes. It is shown in practice in Lorteau et al.[4,5] where the accurate predictions of subsonic (M=0.9) jet noise are obtained on a fully unstructured (tetrahedrons-predominantly) mesh containing only 3.9M elements with the use of third-order DG method implemented in the Aghora CFD solver. Despite the significant progress in jet simulation on unstructured meshes demonstrated in the above papers, due to a large number of degrees of freedom required, the corresponding computations generally remain very costly in the light of industrial applications. Furthermore, a gain of the DG method in accuracy is not evident for supersonic jets when the high accuracy should not be degraded by monotonizing techniques. The recent results on acoustics of supersonic jets presented in Bres et al.[6] mark a way of compromise between accuracy and costs in jet simulation on unstructured meshes. The authors use the unstructured research code CharLES, to simulate a wide range of jets including different parameters and configurations. The compressible solver CharLES exploits a higher-accuracy cell-centered finite-volume scheme based on polynomial reconstructions of variables. The polynomials are quadratic in the face-normal direction remaining linear in the rest two directions.

In the paper, to simulate aeroacoustics of subsonic and supersonic jets on unstructured meshes, we present another higher-accuracy lower-cost numerical algorithm. It is based on quasi-1D vertex-centered EBR (Edge-Based

[1] Researcher, Computational Aeroacoustics Lab, Miusskaya Sq, 4-A.
[2] Head of Lab, Computational Aeroacoustics Lab, Miusskaya Sq, 4-A, Senior AIAA Member.

Reconstruction) schemes[7,8]. These schemes combine the advantages of structured and unstructured methods and can be also considered as a compromise between accuracy and computational costs in jet simulations. On arbitrary unstructured meshes the EBR schemes are theoretically of the second order as highest depending on the types of mesh elements and duals. On tetrahedral meshes with barycentric cells they are exact on linear functions i.e. 1-exact as the scheme of solver CharLES[6]. At the same time, in terms of error values the EBR schemes generally exhibit the accuracy noticeably higher than most traditional second-order schemes. It happens thanks to the special property of EBR schemes to coincide with the high-order finite-difference algorithms on translationally invariant (TI) meshes[8], i.e. "uniform" grid-like tetrahedral or hexahedral meshes which are invariant with respect to translation on its edge-vectors. In particular, on TI-meshes the EBR schemes provide up to the 5th-6th order of accuracy whereas the solver CharLES possesses the 3rd order.

Similarly to Travin et al.[9], we develop a hybrid version of EBR schemes which opens a way to adaptively control the volume of numerical dissipation. Moreover, we equip the method with a possibility to adaptively change the length of quasi-1D approximation stencils depending on local flow parameters and mesh quality. For treating discontinuities in case of jets with shocks we use the quasi-1D WENO techniques[10] and incorporate it to the main hybrid scheme.

A gradual development and enhancement of the hybrid RANS-LES approach DES (Detached Eddy Simulation) significantly expand the frames of its application. The most recent DES formulation[11] has strongly advanced in solving a fundamental problem of the original method which is the so-called "grey area" problem resulting in the delay of "numerical" transition from the steady RANS to unsteady LES solution in shear layers. The acceleration of RANS-to-LES transition and the developed turbulence generation is achieved by the specification of LES subgrid scale. It provides an automatic identification of the initial regions of shear layers and the corresponding reduction of subgrid viscosity in these areas. At the same time, the new SLA (Shear-Layer Adapted) subgrid scale Δ_{SLA} naturally switches to the classical (for LES branch of DES) definition $\Delta = \Delta_{\max} = \max\{\Delta_x, \Delta_y, \Delta_z\}$ in the region of developed turbulent flow. As a result, the method has been extended to the simulation of a wide range of problems where the delay of developed 3D turbulence generation in shear layers causes unacceptably poor accuracy in the prediction of most important ("principal") properties. Jets are a typical demonstrative example of such flows which is considered in the paper. We adapt the hybrid RANS-LES scale-resolving approaches of DES family, including the above mentioned recent one[11] which accelerates RANS-to-LES transition in shear layers, to unstructured meshes and implement them using quasi-1D edge-based vertex-centered schemes.

In the paper we present the predictions both of subsonic and sonic underexpanded jets and examine acoustic fields generated by them. The first case is the subsonic unheated immersed round jet that has been investigated experimentally by Viswanathan[12]. Simulations of this jet have been carried out by Shur et al. on the sequence of refining meshes using both ILES[13] and new enhanced DDES[14] approaches, and the high-fidelity structured numerical algorithm. The second case is the underexpanded hot round jet without co-flow that has been simulated by Shur et al.[15] (case 1a). The results of simulation (far field noise directivity and 1/3-octave spectrums at different observer angles) are compared with the experimental data of Ahuja et al[16,17].

II. Numerical Algorithm

A. RANS-LES Approaches on Unstructured Meshes

The subgrid-scale computation techniques involved to the recent DES formulation[11] are initially proposed for structured meshes and finite-volume methods. We adjust them to the turbulent-flow simulation on unstructured meshes using the edge-based vertex-centered numerical schemes. First, our new development consists in the adaptation of scale $\tilde{\Delta}_{\omega} = 1/\sqrt{3}\max_{i,j}\left|\mathbf{l}_i - \mathbf{l}_j\right|$ that presents a term (see formula (1) in[11]) of the new subgrid scale formulation Δ_{SLA}. Here $\mathbf{l}_i = \mathbf{n}_{\omega} \times \mathbf{r}_i$, $\mathbf{n}_{\omega}$ is the unit vector aligned with the vorticity vector, and under $\mathbf{r}_i$ we assume the radius-vectors of vertices bearing the corresponding dual cell of unstructured mesh. The second term, i.e. the "kinematic part" of the subgrid scale formulation Δ_{SLA} ($F_{KH}\left(<VTM>\right)$ function), remains the same.

Note that the introduction of scale $\tilde{\Delta}_{\omega}$ as compared to the commonly used scale $\Delta_{\max}$ reduces the turbulent viscosity only in the regions of anisotropic cells. In isotropic regions it changes nothing, so that only the "kinematic part" of new subgrid scale contributes to the acceleration of RANS-to-LES transition.

B. Quasi-1D Edge-Based Schemes

Consider the EBR schemes in more details and describe its main properties briefly as applied to the hyperbolic system

$$\frac{\partial \mathbf{Q}}{\partial t} + \nabla \cdot \boldsymbol{\mathcal{F}}(\mathbf{Q}) = 0, \qquad \boldsymbol{\mathcal{F}} = \left(\rho\mathbf{u},\, \rho\mathbf{u}\mathbf{u} + p\mathbf{I},\, (E+p)\mathbf{u}\right)^T \tag{1}$$

written with respect to conservative variables $\mathbf{Q} = \left(\rho, \rho\mathbf{u}, E\right)^T$. Here ρ – density, $\mathbf{u}$ – velocity vector, p – pressure, $\mathbf{I}$ – identity matrix, $\boldsymbol{\mathcal{F}}$ – the flux vector. The general formulation of edge-based vertex-centered schemes can be represented as

$$\left(\frac{d\mathbf{Q}}{dt}\right)_i = -\frac{1}{v_i}\sum_{j\in N_1(i)} \mathbf{h}_{ij}\left|\mathbf{n}_{ij}\right|, \tag{2}$$

where v_i – the volume of the dual cell built around vertex i, $N_1(i)$ – a set of first-level neighbors of node i, $\mathbf{h}_{ij}$ – the numerical flux which is calculated as $\mathbf{h}_{ij} = \boldsymbol{\mathcal{F}}_{ij}\cdot\mathbf{n}_{ij}\big/\left|\mathbf{n}_{ij}\right|$, $\mathbf{n}_{ij} = \int_{\partial C_{ij}} \mathbf{n}\, ds$, ∂C_{ij} – the boundary of cell interface between nodes i and j, $\mathbf{n}_{ij}$ – the oriented square of cell surface C_{ij}. A key point in the formulation (2) of EBR schemes is that both the numerical flux $\mathbf{h}_{ij}$ and the oriented square $\mathbf{n}_{ij}$ are evaluated at the edge ij midpoint only. A specific scheme of the EBR family is defined by the method of calculating flux $\mathbf{h}_{ij}$ on an extended edge-based quasi-1D stencil. We calculate $\mathbf{h}_{ij}$ as a solution of approximate Godunov-type Riemann solver or flux-splitting methods basing on the left and right states $\mathbf{F}_{ij,}^{L/R}$ $\mathbf{F} = \boldsymbol{\mathcal{F}}_x n_x + \boldsymbol{\mathcal{F}}_y n_y + \boldsymbol{\mathcal{F}}_z n_z$ or/and $\mathbf{Q}_{ij}^{L/R}$ which, in their turn, are determined with the use of quasi-1D reconstructions. The reconstructions are built in a way that they transform to the corresponding high-order finite-difference approximations when applied to uniform grid-like (or TI) meshes. Further we denote an EBR scheme as EBRn scheme if its highest theoretical order (which is reachable on TI meshes) is equal to n.

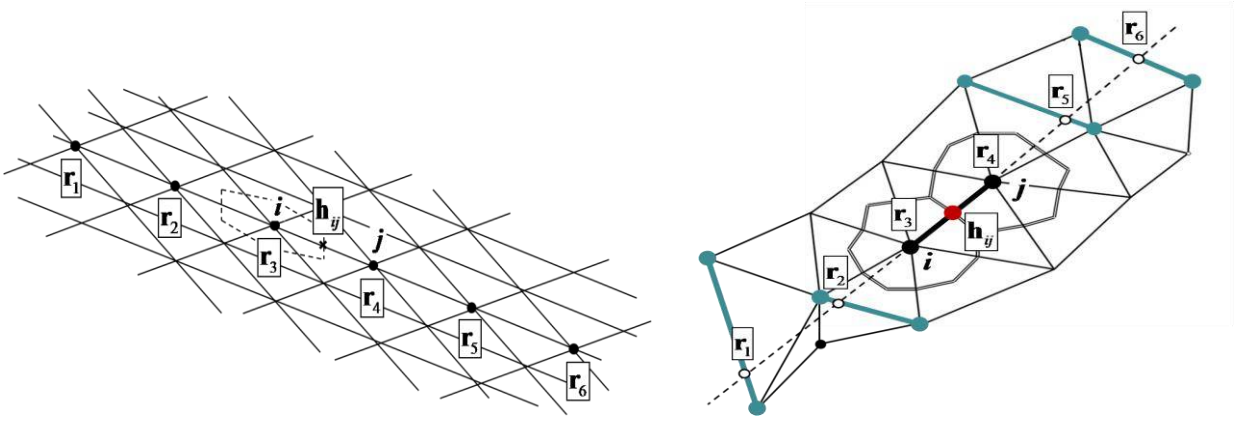

Figure 1. Quasi-1D stencils of EBR schemes: on TI-mesh (left), on arbitrary triangular mesh (right).

Figure 1 schematically shows the extended quasi-1D edge-based stencil we use for the numerical flux evaluation on a triangular unstructured mesh. The reconstructions for calculating the left and right states involve the values in the points with local numeration $\{\mathbf{r}_i\}$, $i = \overline{1,6}$. The values in the points that do not coincide with the mesh vertices are determined with the help of linear interpolation on the correspondent edges which are intersected by the edge ij direction. In 3D, the reconstructions of left and right states are built in a similar way with replacing the intersected edges with the intersected faces. In particular, in the EBR5 scheme the reconstruction operators $\mathbb{R}_{ij}^{L/R}$ acting on mesh function ψ can be written in terms of divided differences $\Delta\psi_{i+1/2} = \left(\psi_{i+1} - \psi_i\right)\big/\Delta r_{i+1/2}$, $\Delta r_{i+1/2} = \left|\mathbf{r}_{i+1} - \mathbf{r}_i\right|$ as

$$\mathbb{R}_{ij}^{L}\left(\{\psi\}\right)=\psi_i+\frac{\Delta r_{7/2}}{2}\left(-\frac{1}{15}\Delta\psi_{3/2}+\frac{11}{30}\Delta\psi_{5/2}+\frac{4}{5}\Delta\psi_{7/2}-\frac{1}{10}\Delta\psi_{9/2}\right)$$
$$\mathbb{R}_{ij}^{R}\left(\{\psi\}\right)=\psi_j-\frac{\Delta r_{7/2}}{2}\left(-\frac{1}{15}\Delta\psi_{11/2}+\frac{11}{30}\Delta\psi_{9/2}+\frac{4}{5}\Delta\psi_{7/2}-\frac{1}{10}\Delta\psi_{5/2}\right). \quad (3)$$

All the stencils and metrical coefficients which provide the algorithm are determined at the preprocessing stage and the total required costs of EBR schemes appear not significantly higher than in the case of "traditional" second-order finite-volume methods. Another remarkable detail is that the algorithm allows to easily change a width of the reconstruction stencil in dependence on flow and mesh local characteristics, and thereby to control the scheme dissipation. We exploit this property to compute the jets.

For the time integration in the jet cases presented in the paper we use the fourth-order explicit Runge-Kutta scheme.

C. Shock Capturing

To treat possible discontinuities and solutions with high gradients, we equip the EBR schemes with the quasi-1D WENO techniques.[10] To implement shock capturing, we mostly use the Riemann solver of Roe written in characteristic variables to which we apply the WENO-reconstruction in concordance with the classical finite-difference WENO scheme.[18] In doing so, in our quasi-1D unstructured case, we represent the involved lower-order reconstructions and corresponding smoothness monitors in terms of divided differences along the 1D-stencils (Fig.1). The resulting WENO-reconstruction operator $\mathbb{R}_{ij}^{WENO,\,L}$ as applied to the left state of mesh function ψ is given by the following formulas:

$$\mathbb{R}_{ij}^{WENO,\,L}\left(\{\psi\}\right)=\psi_i+\sum_{k=1}^{3}\omega^{L,\,k}\;\mathbb{R}_{ij}^{L,\,k}\left(\{\psi\}\right),$$
$$\mathbb{R}_{ij}^{L,\,1}\left(\{\psi\}\right)=\frac{\Delta r_{7/2}}{2}\left(-\frac{2}{3}\Delta\psi_{3/2}+\frac{5}{3}\Delta\psi_{5/2}\right),$$
$$\mathbb{R}_{ij}^{L,\,2}\left(\{\psi\}\right)=\frac{\Delta r_{7/2}}{2}\left(\frac{1}{3}\Delta\psi_{5/2}+\frac{2}{3}\Delta\psi_{7/2}\right), \quad (4)$$
$$\mathbb{R}_{ij}^{L,\,3}\left(\{\psi\}\right)=\frac{\Delta r_{7/2}}{2}\left(\frac{4}{3}\Delta\psi_{7/2}-\frac{1}{3}\Delta\psi_{9/2}\right)$$

with the weights $\omega^{L,\,k}$: $\omega^{L,\,k}=\dfrac{\sigma^{L,\,k}}{\sum_{k=1}^{3}\sigma^{L,\,k}}$, $\sigma^{L,\,k}=\dfrac{\Omega^k}{\left(10^{-10}+IS^{L,\,k}\right)^2}$, $\Omega^1=\dfrac{1}{10}$, $\Omega^2=\dfrac{6}{10}$, $\Omega^3=\dfrac{3}{10}$ which are defined in dependence on smoothness monitors $IS^{L,\,k}$:

$$IS^{L,\,3}=\frac{13}{12}\left(\Delta\psi_{5/2}-\Delta\psi_{3/2}\right)^2+\frac{1}{4}\left(3\Delta\psi_{5/2}-\Delta\psi_{3/2}\right)^2,$$
$$IS^{L,\,2}=\frac{13}{12}\left(\Delta\psi_{7/2}-\Delta\psi_{5/2}\right)^2+\frac{1}{4}\left(\Delta\psi_{7/2}+\Delta\psi_{5/2}\right)^2, \quad (5)$$
$$IS^{L,\,3}=\frac{13}{12}\left(\Delta\psi_{9/2}-\Delta\psi_{7/2}\right)^2+\frac{1}{4}\left(\Delta\psi_{9/2}-3\Delta\psi_{7/2}\right)^2.$$

D. Hybrid Scheme

As is known, to provide correct turbulent-flow predictions, the scale resolving approaches require a carefully-calibrated balance between the numerical dissipation and instability. A reduction of numerical dissipation at the initial region of shear layers is a crucial point. In these areas a scheme should be both accurate and stable enough, to allow for a correct representation of arising small physical instabilities and damping "parasitic" numerical oscillations. The same scheme properties should be maintained in the regions of developed turbulence which are responsible for the noise generations mechanisms. Along with that, in the areas where the turbulent viscosity goes down a proper representation of the acoustic waves that propagate towards the FWH surfaces needs in some extra

dissipation, in order to avoid possible numerical instability. To meet the above peculiarities, one suggests to use the hybrid schemes that combine upwind and central-difference parts for the numerical-flux evaluation[6,9,15,19].

A presence of shocks in the regions of developed turbulence strongly complicates the process of building an appropriate robust hybrid scheme that should control an optimal blending of central-difference, upwind and shock-capturing approximations. We design the following three-term hybrid formulation for calculating the reconstructed values:

$$\mathbb{R}_{ij}^{HYBRID,\,L}\left(\{\psi\}\right)=\sigma^3\mathbb{R}_{ij}^{WENO,\,L}\left(\{\psi\}\right)+(\sigma-\sigma^3)\mathbb{R}_{ij}^{L}\left(\{\psi\}\right)+(1-\sigma)\frac{\mathbb{R}_{ij}^{L}\left(\{\psi\}\right)+\mathbb{R}_{ij}^{R}\left(\{\psi\}\right)}{2} \tag{6}$$

where reconstructions $\mathbb{R}_{ij}^{WENO,\,L}\left(\{\psi\}\right)$ and $\mathbb{R}_{ij}^{L}\left(\{\psi\}\right)$, $\mathbb{R}_{ij}^{R}\left(\{\psi\}\right)$ are defined in (4) and (3) correspondingly, $\sigma \in [0,1]$ is the weight coefficient of upwind component of the hybrid scheme proposed by Travin et al.[9]. According to (6), the central-difference reconstruction and the corresponding numerical flux dominate when σ varies near zero, the upwind (with no limiters) reconstruction is working when σ is of moderate values and the WENO reconstruction gets involved when σ approaches to 1.

A development of robust and effective sensor for a shock-capturing scheme is still a challenging problem. For instance, different techniques are presented in Johnsen et al [19]. Some other methods are developed for scale-resolving simulation of turbulent flows with strong gradients[6,15]. For the jet predictions we use a rather simple sensor which is proposed in Shur et al.[15] (see equation (1)). It is based on a difference between the pressure values in two adjacent nodes. The WENO reconstruction weight is set equal to 1 when the maximum value of $\left|p_{i+1}-p_i\right|/\min\left\{p_i,p_{i+1}\right\}$, where p_i, p_{i+1} are the pressure values in two neighboring points, exceeds 0.3 on the stencil consisting of up to 5 points. This sensor is well activated at the shocks and does not contaminate the resolved turbulence region. Its work is demonstrated below in the sonic underexpanded hot jet case.

E. Far-Field Noise Prediction

To predict far-field acoustics, we use the Lighthill acoustic analogy in the form of a modified version of the integral Ffowcs Williams and Hawkings (FWH) method[20] in terms of retarded times. According to Shur et al.[21,22] the data for acoustical postprocessing is accumulated on the nested closed permeable control surfaces excluding the "quadrupole" volume terms. We apply the density-by-pressure substitution assuming the isentropic relations and the outflow-discs[21] and conical "sleeve" surfaces[23] averaging techniques applying for reduction of spurious noise.

III. Subsonic Jets

A. Problem Formulation and Computational Setup

Consider the immersed unheated subsonic (Mach number $M_{jet}=0.9$) round jet with Reynolds number $\mathrm{Re}_D=1.1\cdot10^6$ based on nozzle diameter D. The computational setup is provided by M. Shur and M. Strelets from Peter the Great St.Petersburg Polytechnic University and fully corresponds to the papers[13,15]. It includes the preliminarily RANS-computed profiles which are imposed at the nozzle exit as inflow boundary conditions with no special excitation for accelerating the RANS-to-LES transition. Such two-stages approach[24] (nozzle and jet-plume computation using RANS at the first stage, jet-plume computation using LES at the second stage) reduces the computational costs due to the moderate requirements on boundary layer resolution and the wall-normal mesh steps. At the same time, it allows to reproduce realistic thin-boundary-layer properties at the nozzle exit that are inherent in high-Reynolds flows. Within this approach a fast transition to resolved turbulence in the shear layers crucially depends both on the subgrid LES model and the numerical-scheme dissipation.

The computations are carried out using the sequence of three refining high-quality axisymmetric meshes which contain 1.52 M, 4.13 M and 8.87 M vertices (Grid 1, Grid 2 and Grid 3, correspondingly). They have 64, 80 and 160 cells in azimuthal direction. More details on the mesh parameters are described in the paper[13]. The patterns of Grid 1 in the meridian plane are presented in Figure 2. The edges inside the jet-plume region are colored by the vorticity magnitude. The FWH control surfaces are indicated in magenta. Notice that the Grid 2 and Grid 3 differ only in the resolution in the azimuthal direction.

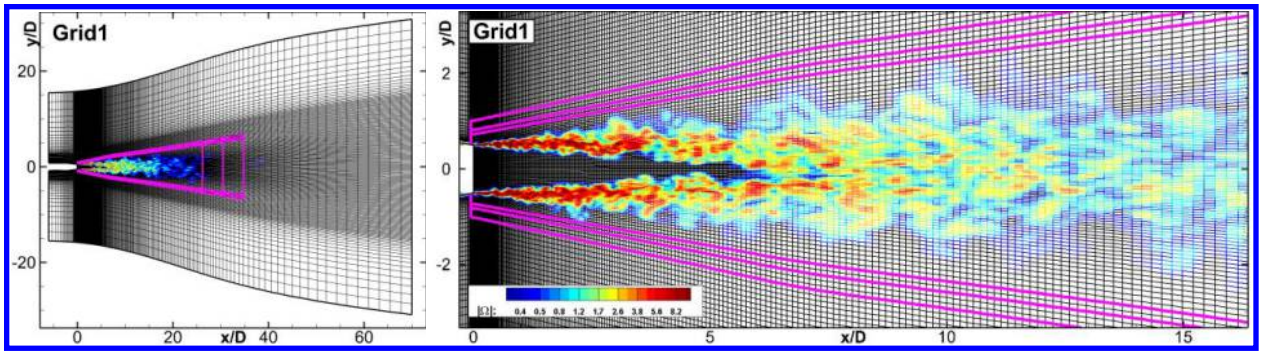

Figure 2. Computational mesh patterns in meridian plane for subsonic jet (Grid 1). Mesh edges in the jet plume region are colored by vorticity magnitude. FWH control surfaces are colored in magenta.

A physical time of computation is about 700 D/U_{jet}. A mature turbulent flow is developed approximately by time $400D/U_{jet}$. Then, for time 300 D/U_{jet} we accumulate the near-field statistics and the data on FWH control surfaces for far-field acoustics postprocessing. The profiles of the lipline distributions and radial profiles shown below are averaged over the azimuthal direction under the assumption of jet axial symmetry.

The far field signals are estimated at distance 98D from the center point at the nozzle exit. For obtaining less "noisy" 1/3-octave integrated sound pressure levels (SPL), the power spectra of signals at 32 equidistant points along the azimuthal direction are averaged for each observer angle.

B. Numerical Results and Analysis

Figure 3 presents 3D visualizations of jet-plume region using Q-criterion for the three refining meshes. It is seen that the shear layers develop practically with no delay even on the coarse computational mesh (Grid 1). Figure 2 confirms this fact and an efficiency of the recent DDES approach in general. Moreover, the characteristic sizes of resolved turbulent structures are in a good agreement with the corresponding results obtained with the use of high-fidelity low-dissipation numerical algorithm on structured meshes presented in Shur et al.[11]

The evaluation of the numerical results includes the comparison of near field turbulence characteristics with the experimental data[25-29] for subsonic jets of similar parameters and configurations. The corresponding comparison is given in Figures 5 and 6. An obvious trend is that the results converge with the mesh refinement. Note that the distributions of streamwise-velocity fluctuations and peak Reynolds stresses are predicted correctly even using the coarse mesh.

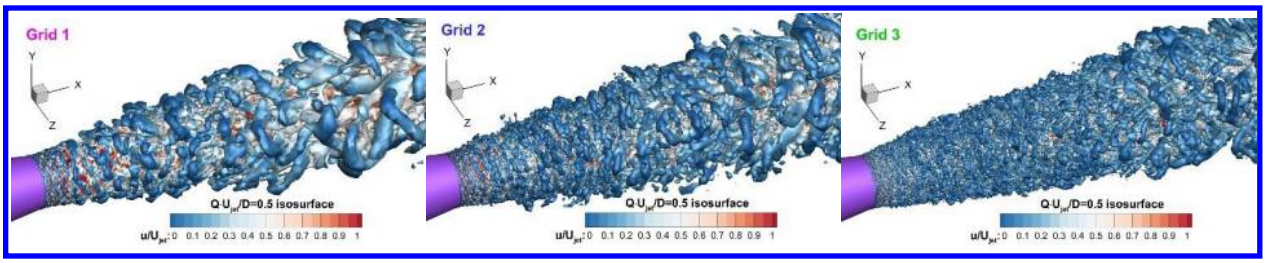

Figure 3. Flow patterns of subsonic round jet: Q-criterion isosurfaces colored by streamwise velocity.

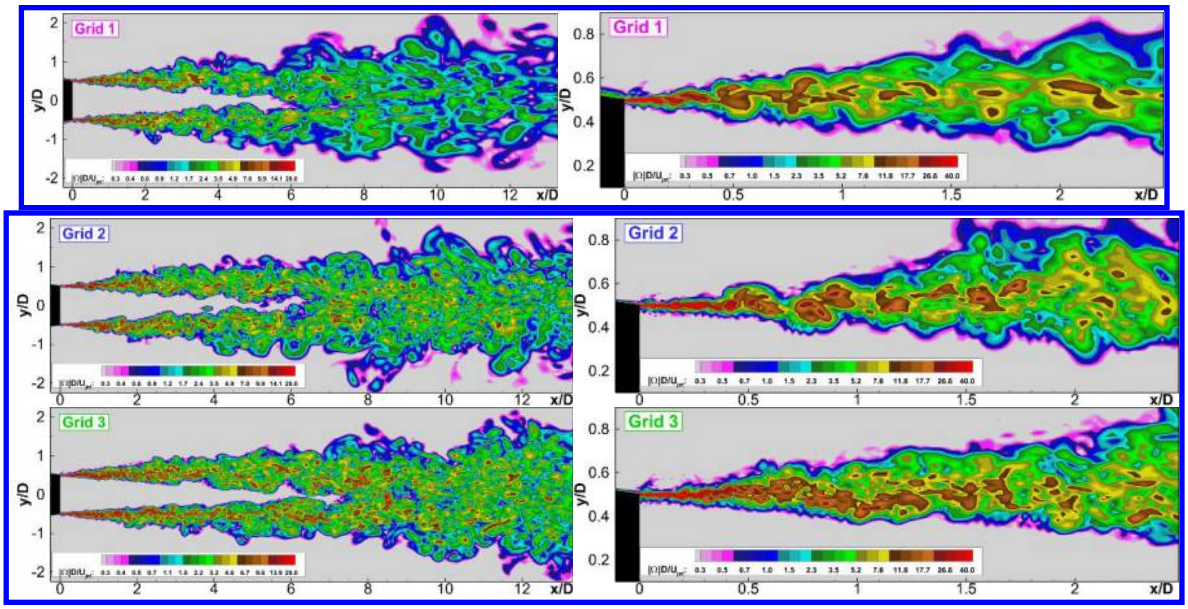

Figure 4. Subsonic jet: vorticity magnitude distribution in meridian plane (left) and zoomed near the nozzle exit edge.

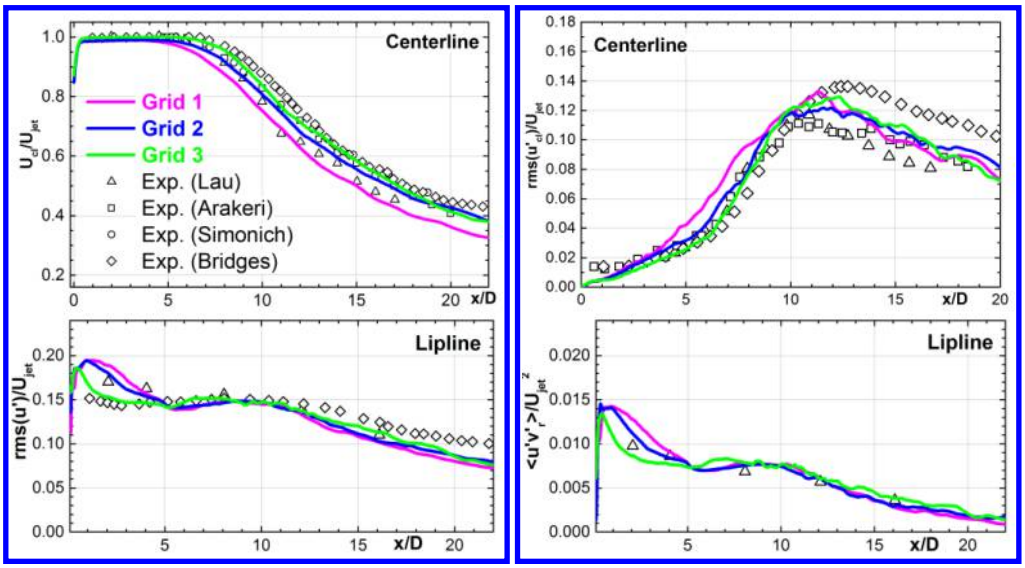

Figure 5. Subsonic jet: distributions of streamwise velocity and root mean square value of its pulsation component along centerline (top) and peak Reynolds stresses along lipline (bottom) compared with experiments of similar jet of Lau[25,26], Arakeri[27], Simonich[28] and Bridges[29].

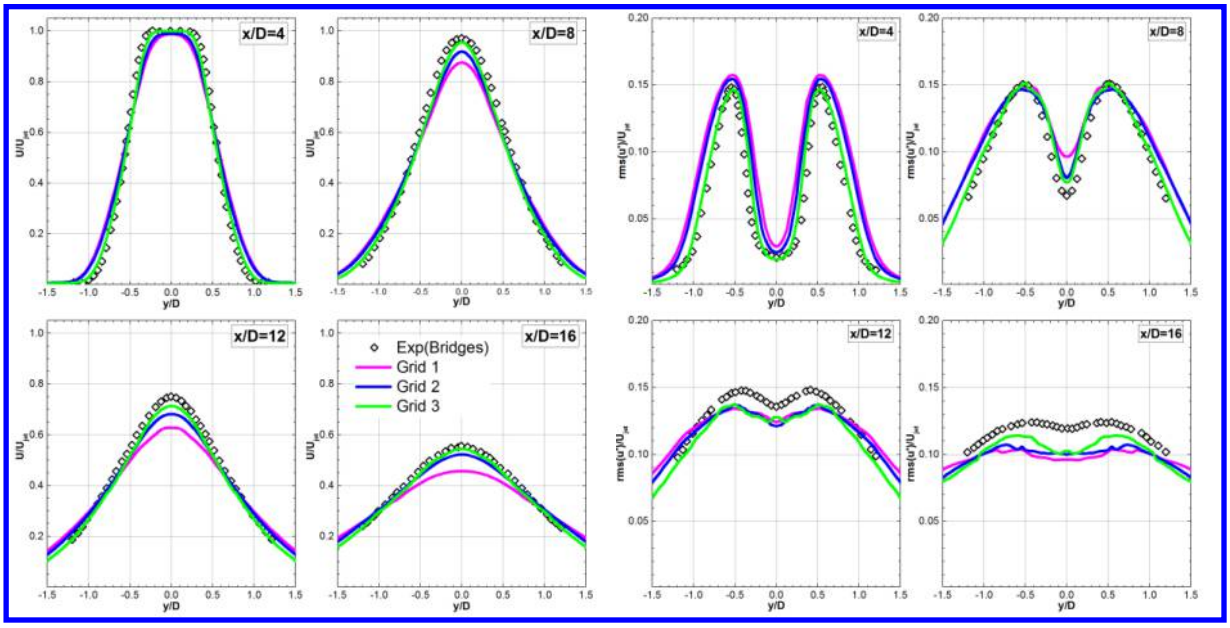

Figure 6. Subsonic jet: profiles of averaged streamwise velocity (left) and root mean square values of its pulsation component compared with experimental data of Bridges[29].

Figure 7 presents a snapshot of pressure time-derivative distribution that shows the acoustic field obtained on Grid 3. The concentric acoustic waves coming from the jet potential core are clearly seen. At the same, the disturbances crossing the FWH surfaces at $7<x/D<17$ seem of non-physical nature. They may be generated due to a lack of dissipation of the numerical scheme.

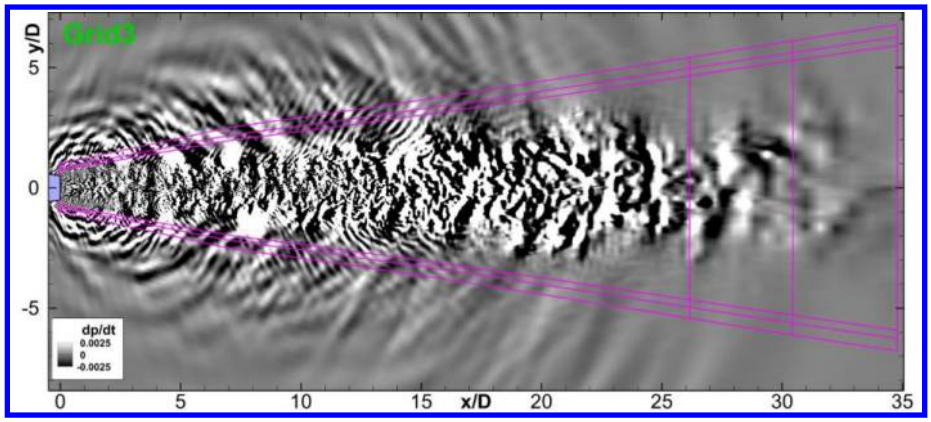

Figure 7. Subsonic jet: instantaneous flow field of pressure time derivative.

Figures 8 and 9 show the overall sound pressure level (OASPL) distributions versus the observer angle and 1/3-octave spectra in the far field points at different observer angles in comparison with the corresponding experiment data[12]. It is seen that the mesh refinement provides the convergence and a better agreement with the reference data.

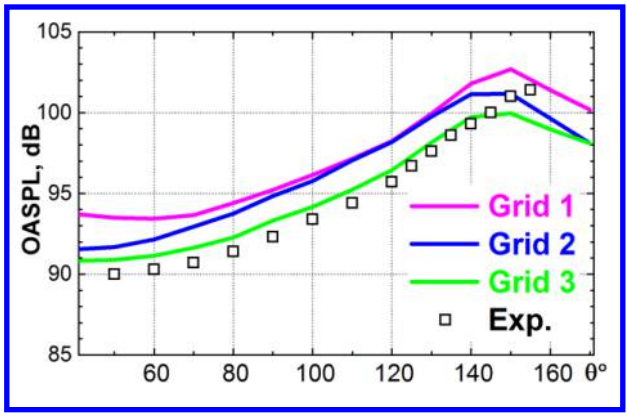

Figure 8. Subsonic jet farfield acoustics: noise directivity compared with experiment[12].

Note that the use of unstructured quasi-1D method does not lead to some significant far-field noise contamination that can appear due to numerical oscillations caused by possible instabilities of the low-dissipative scheme. It is important since, unlike mean turbulent-flow characteristics, jet aeroacoustics is sensitive to non-physical waves that can occur in the solution. The obtained results demonstrate a

plausible jet prediction thanks largely to an accurate simulation of the initial parts of jet shear layers and the early RANS-to-LES transition.

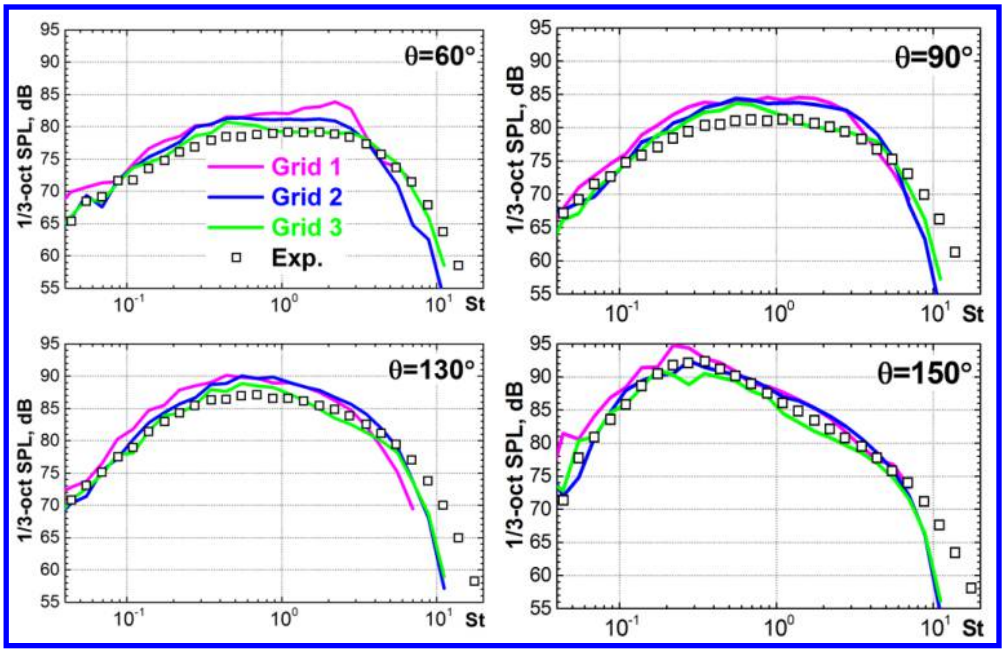

Figure 9. Subsonic jet farfield acoustics: 1/3-octave spectrums compared with experiment[12].

IV. Underexpanded hot jet

A. Problem Formulation and Computational Setup

The free sonic underexpanded hot jet that has been investigated experimentally by Ahuja et al.[16,17] and simulated using ILES approach by Shur et al.[15] is considered. The jet with diameter $D = 2.54$ cm exhausts into the room characterized by following parameters: $P_\infty = 1.013 \cdot 10^5$ Pa, $T_\infty = 293$ K, $\rho_\infty = 1.2$ kg/m^3. The nozzle pressure ratio (NPR) and nozzle temperature ratio (NTR) are equal to 3.86 and 2.97 correspondingly. Reynolds number based on fully expanded jet flow velocity $U_{jet}^{FE} = 748.4$ m/s (it is referred as U_{jet} below) and nozzle exhaust diameter $\mathrm{Re}_D = 1.2692 \cdot 10^6$. The corresponding "acoustic" Mach number $M_a^{FE} = U_{jet}^{FE} / c_\infty = 2.18$ (c_∞ is ambient speed of sound).

As for the subsonic jet, the computational setup including the mesh and the preliminary RANS-computed nozzle exit profiles are provided by M. Shur and M. Strelets. The computational mesh in use that is plotted in Figure 10 consists of 4.55M nodes. It has 80 cells in the azimuthal direction.

A physical time of the computation is 450 D/U_{jet}. A mature turbulent flow is developed approximately by time 150$D/$U$_{\mathrm{jet}}$. For the next time 300 D/U_{jet}, the near-field statistics and the data on the FWH control surfaces for the far-field acoustics postprocessing are accumulated. The same techniques to obtain statistically converged results as for the subsonic jet case are applied. In order to avoid possible reflections of sound waves from the outer boundary, the sponge layer method[21] is used.

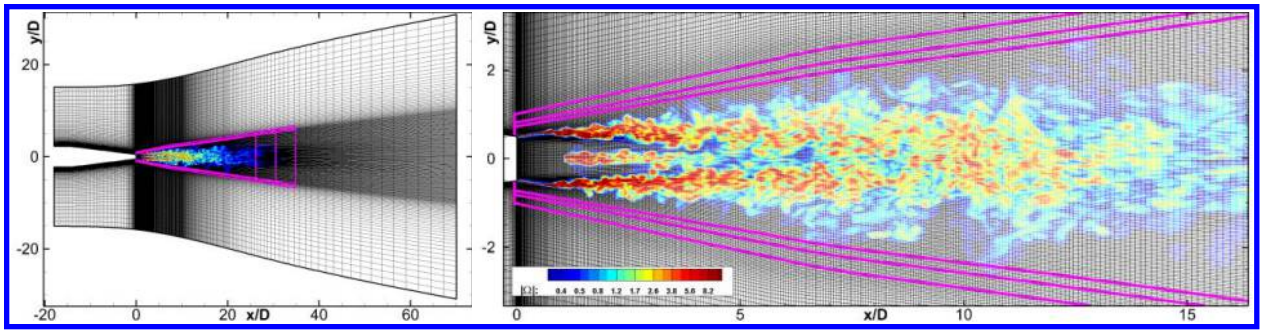

Figure 10. Computational mesh patterns in meridian plane for underexpanded hot jet. Jet plume region is colored by vorticity magnitude. FWH control surfaces are marked in magenta.

B. Numerical Results and Analysis

Figure 11 presents a snapshot characterizing the resolved turbulent structures in the jet plume together with the generated acoustic waves. The predicted shear layers look very close to the reference simulation[15]. Figure 12 (top) shows the instantaneous and averaged Mach number fields. One can see the shock cells which are specific for imperfectly expanded jets, the Mach disc formed behind the first shock cell and the internal downstream-developed shear layer. In Figure 12 (bottom) both instantaneous and averaged fields of density gradient magnitude ("numerical shchliren") are demonstrated. The edges where the hybrid scheme uses the pure WENO reconstructions are marked in red. The picture illustrates a good work of the sensor we use. It satisfies the following requirements: it is activated at the shocks and do not work in the resolved-turbulence region where too dissipative WENO scheme may damp the solution.

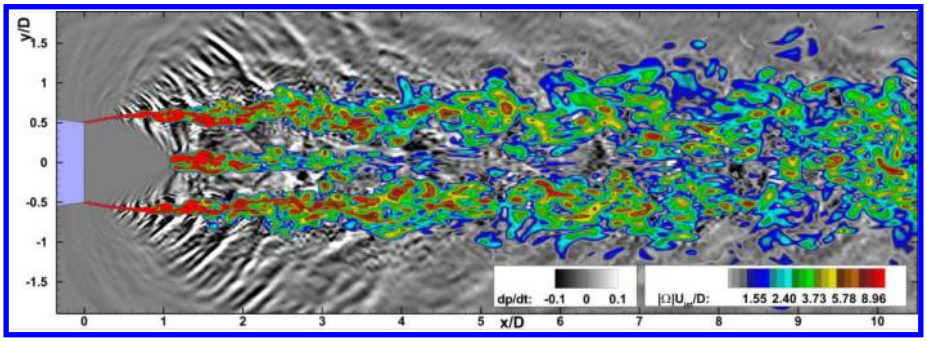

Figure 11. Underexpanded hot jet: instantaneous flow fields of vorticity magnitude and pressure time derivatives.

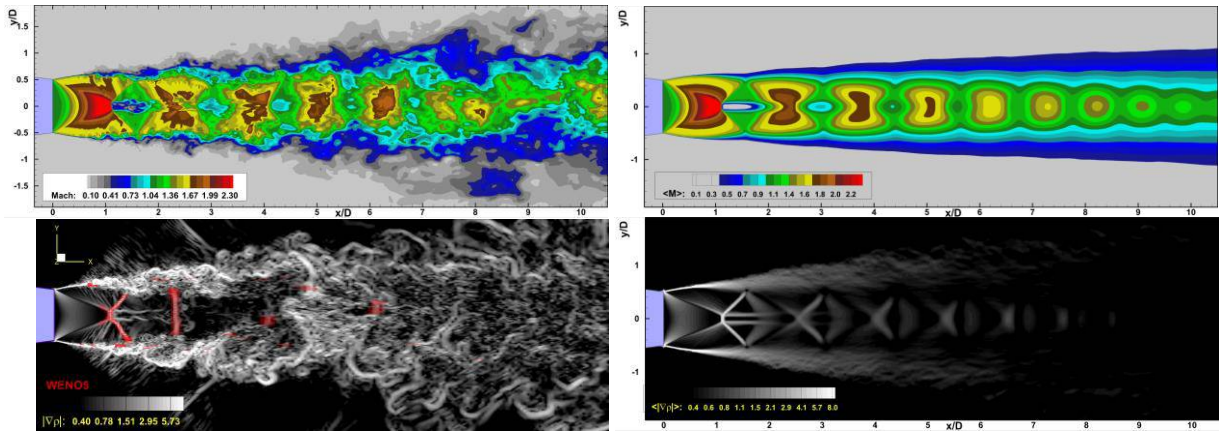

Figure 12. Underexpanded hot jet: instantaneous (left) and averaged (right) distributions of Mach number (top) and density gradient (numerical schlieren) (bottom). Edges where pure WENO5 reconstruction is used are marked in red.

The sound wave patterns of different nature and directions of propagation which are generated by the underexpanded hot jet are distinctively seen in Figure 13. The strongest ones are high-frequency Mach waves

generating in the initial region of the jet shear layer and propagating predominantly at the angles of high emission. The presence of concentric wave patterns corresponds to the broadband shock cell (BBSC) noise generating by the interaction of shock cells with the turbulence. As in the case of subsonic jet, "numerical" oscillations are noticeable especially in Figure 13, right in the region $10<x/D<20$.

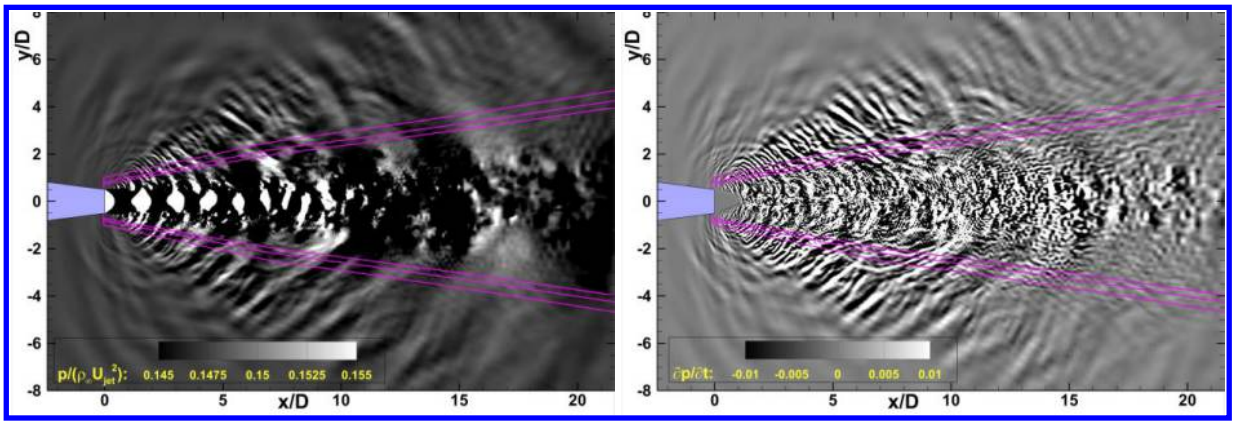

Figure 13. Underexpanded hot jet: instantaneous flow fields of pressure and its time derivative.

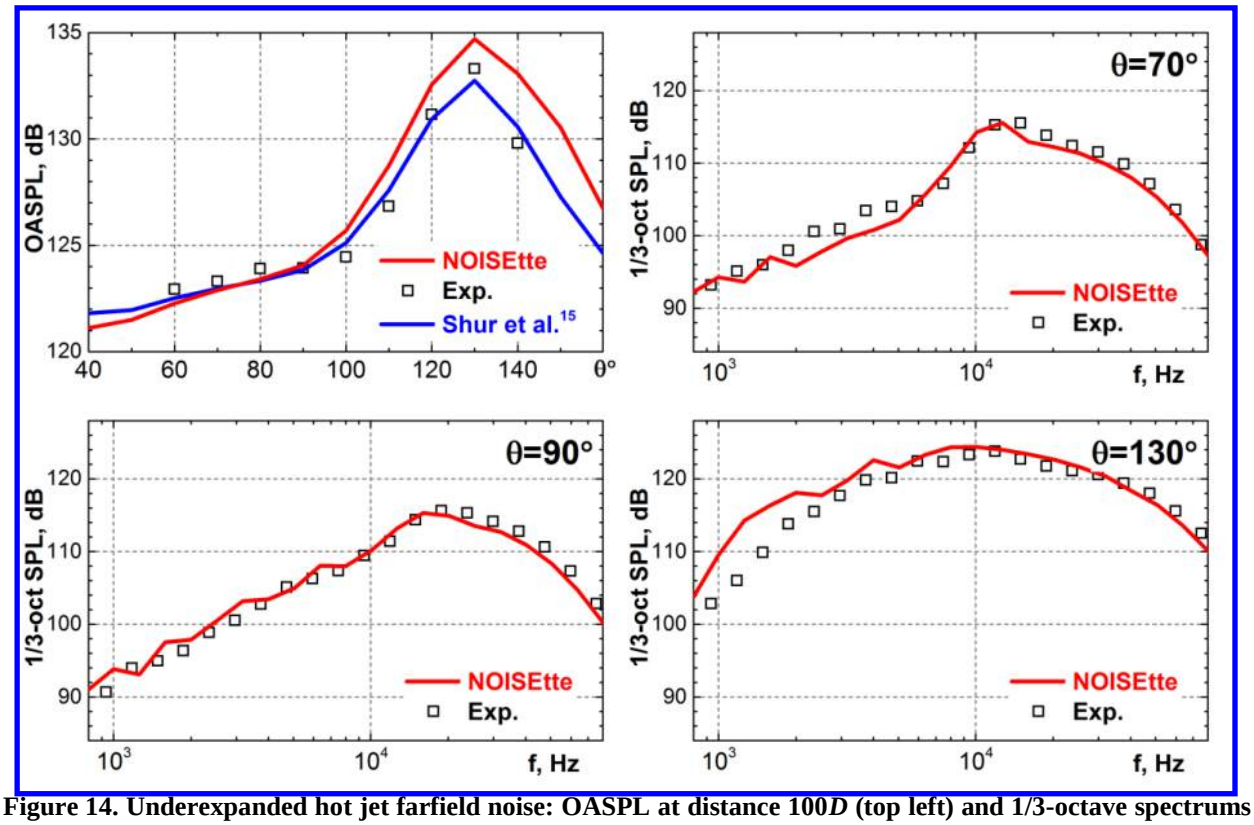

Figure 14. Underexpanded hot jet farfield noise: OASPL at distance 100*D* (top left) and 1/3-octave spectrums at different observer angles compared with experiment[16,17] and reference computation[15].

Figure 14 shows the noise directivity at distance 100*D* and 1/3-octave spectra at different observer angles. The acoustics results in far field are well correlated with the reference data. A noticeable overestimation of OASPL at the high observer angles and 1/3-octave sound pressure levels at $\theta = 130°$ for lower frequencies may be caused by non-physical numerical oscillations and need in further investigations.

V. Conclusion

In the paper we show the capacity of quasi-1D edge-based vertex-centered schemes as applied to simulating jet

aerodynamics and jet aeroacoustics. The advantages of the numerical algorithm presented is its higher accuracy in comparison with most second-order schemes and lower costs in comparison with very high-order methods.

The results we obtain contribute to accurate predictions of jets in complex industrial configurations where the use of unstructured meshes (at least, partly unstructured) is fully justified. It should be noted that the jet predictions presented in the paper have been carried out on jet-consistent structured meshes with the use of the unstructured algorithm. The corresponding simulations on fully unstructured meshes are under way.

The future developments of our numerical algorithm will be mostly aimed at improving its robustness and providing its better dynamic adaptability to the flow and mesh peculiarities.

Acknowledgments

The research is supported partly by the Russian Science Foundation (Project 16-11-10350) and Russian Foundation for Basic Research (Project 15-01-07911). Project 16-11-10350 includes the developments of DES-family models on unstructured meshes, while Project 15-01-07911 elaborates the quasi-1D higher-accuracy schemes.

All the predictions have been performed with the use of in-house code NOISEtte. Supercomputers Lomonosov-2 of Moscow State University, MVS-10P of Joint Supercomputer Center of RAS, HPC4 of Kurchatov Institute have been used for the computations. The authors thankfully acknowledge these institutions.

The authors thank M. Shur and M. Strelets for the helpful discussions, advices and the data for jet cases, and our colleague P. Bakhvalov for the useful technical recommendations and comments.

References

[1]Lupoglazoff N. and Vuillot F., Recent progress in numerical simulations for jet noise computation using LES on fully unstructured meshes, AIAA Paper 2015-2369.

[2]Tyacke J., Naqavi I., Wang Z., Tucker P., Boehning P., "Predictive LES for Jet Aeroacoustics: Current Approach and Industrial Application", *ASME. Turbo Expo: Power for Land, Sea, and Air, Volume 2A: Turbomachinery*,V02AT41A003.

[3]Mahak M., Naqavi I.Z., Tucker P.G., "Cost-effective hybrid RANS-LES type method for jet turbulence and noise prediction", *International Journal of Aeroacoustics*, Vol 16, Issue 1-2, pp. 97- 111.

[4]Lorteau M., Clero F. and Vuillot F., "Analysis of noise radiation mechanisms in hot subsonic jet from a validated LES solution", *Physics of Fluids*, Vol. 27., 075108 (2015).

[5]Lorteau M., de la Llave Plata M. and Couaillier V., "Turbulent jet simulation using high-order DG methods for aeroacoustics analysis", 11th International ERCOFTAC Symposium on Engineering Turbulence Modelling and Measurements (ETMM11) Proceedings, 2015.

[6]Brès G.A., Ham F.E., Nichols J.W., and Lele S.K., "Unstructured Large-Eddy Simulations of Supersonic Jets", *AIAA Journal*, Vol. 55, No. 4 (2017), pp. 1164-1184.

[7]Koobus B., Alauzet F., Dervieux A., "Computational Fluid Dynamics", Ed. by Magoules F., *CRC Press*, (2011), 131–204.

[8]Abalakin I., Bakhvalov P., Kozubskaya T., "Edge-based reconstruction schemes for unstructured tetrahedral meshes", *Int. Journal for Num. Meth. in Fluids*, 81:6 (2016), 331–356.

[9]Travin A., Shur M., Strelets M., Spalart P.R., "Physical and numerical upgrades in the Detached-Eddy Simulation of complex turbulent flows", *Fluid Mechanics and its Applications*, 65, 239-254. Advances in LES of Complex Flows, R. Friederich and W. Rodi (editors), Kluwer Academic Publishers, (2004).

[10]Abalakin I., Bakhvalov P., Kozubskaya T., "Edge-Based Methods in CAA", *In "Accurate and Efficient Aeroacoustic Prediction Approaches for Airframe Noise", Lecture Series* 2013-03, Ed. by C.Schram, R.Denos, E.Lecomte, von Karman Institute for Fluid Dynamics, (2013).

[11]Shur M., Spalart P., Strelets M., Travin A., "An Enhanced Version of DES with Rapid Transition from RANS to LES in Separated Flows", *Flow Turbul. Combust.*, 95:4 (2015), 709-737.

[12]Viswanathan K., "Aeroacoustics of hot jets", *J. Fluid Mech.*, 516 (2004), 39-82.

[13]Shur M.L., Spalart P. R., Strelets M.Kh., "LES-based evaluation of a microjet noise reduction concept in static and flight conditions", *Journal of Sound and Vibration*, 2011, vol. 330, pp. 4083-4097.

[14]Shur M., Spalart P.R., Strelets M., "Jet noise computation based on enhanced DES formulations accelerating the RANS-to-LES transition in free shear layers", *Int. J. Aeroacoust.*, 15:6-7 (2016), 595-613.

[15]Shur M.L., Spalart P.R., Strelets M.Kh., "LES-based noise prediction for unexpanded jets shocked jets in static and flight conditions", *AIAA Journal*, 2011, v.49, No.9, pp. 2000-2017.

[16]Ahuja, K. K., Tanna, H. K., and Tester, B. J., "Effect of Simulated Forward Flight on Jet Noise, Shock Noise and Internal Noise," *AIAA Paper* 1979-0615, March 1979.

[17]Ahuja, K. K., Tanna, H. K., and Tester, B. J., "The Free Jet as a Simulator of Forward Velocity Effects on Jet Noise," *NASA CR-3056*, Oct. 1978.

[18]Shu C.-W., "Essentially Non-Oscillatory and Weighted Essentially Non-Oscillatory Schemes for Hyperbolic Conservation Laws: *Tech. Rep.: 97-65, NASA*, 1997.

[19]Johnsen, E., et al., "Assessment of High-Resolution Methods for Numerical Simulations of Compressible Turbulence with Shock Waves," *Journal of Computational Physics*, Vol. 229, No. 4, 2010, pp. 1213–1237.

[20]Ffowcs Williams, J.E., Hawkings, D.L., "Sound Generated by Turbulence and Surfaces in Unsteady Motion", *Philos. T. Roy. Soc. A.* A264 (1151), 1969, pp. 321-342.

[21]Shur M.L., Spalart P.R., Strelets M.Kh., "Noise prediction for increasingly complex jets. Part I, Methods and tests; Part II, Applications", *Int J Aeroacoust* 2005, 4: 213–266.

[22]Spalart P.R. and Shur M.L., "Variants of the Ffowcs Williams–Hawkings equation and their coupling with simulations of hot jets", *Int J Aeroacoust* 2009; 8: 477–492.

[23]Y. Khalighi, F. Ham, J. Nichols, S. Lele, and P. Moin, "Unstructured Large Eddy Simulation for Prediction of Noise Issued from Turbulent Jets in Various Configurations", *17th AIAA/CEAS Aeroacoustics Conference*.

[24]Shur M.L., Spalart P.R., Strelets M.Kh., Garbaruk A.V., "Analysis of jet-noise-reduction concepts by large-eddy simulation", *Int J Aeroacoust* 2007, 6: 243–285.

[25]Lau, J.C., Morris, P.J., Fisher, M.J., "Measurements in subsonic and supersonic free jets using a laser velocimeter", *Journal of Fluid Mechanics*, 1979, 93, 1–27.

[26]Lau, J.C., "Effects of exit Mach number and temperature on mean-flow and turbulence characteristics in round jets", *Journal of Fluid Mechanics*, 1981, 105, 193-218.

[27]Arakeri, V.H., Krothapalli, A., Siddavaram, V., Alkislar, M.B., Lourenco, L.M., "On the use of microjets to suppress turbulence in a Mach 0.9 axisymmetric jet", *Journal of Fluid Mechanics*, 2003, 490, 75-98.

[28]Simonich, C., Narayanan, S., Barber, T.J., Nishimura, M., "Aeroacoustic characterization, noise reduction and dimensional scaling effects of high subsonic jets", *AIAA Journal*, 2001, 39(11), 2062-2069.

[29]Bridges, J, Wernet, M.P., "Establishing Consensus Turbulence Statistics for Hot Subsonic Jets", *AIAA Paper* 2010-3751.